Selectivity Map for the Late Stages of CO and CO_2 Reduction to C_2 Species on Cu Electrodes

Oriol Piqué,[a, †] Qi Hang Low,[b, †] Albertus D. Handoko,[c] Boon Siang Yeo,[b,*] and Federico Calle-Vallejo[a,*]

†These authors contributed equally to this work

[a] Oriol Piqué and Dr. Federico Calle-Vallejo
Departament de Ciència de Materials i Química Física & Institut de Química Teòrica i Computacional (IQTCUB), Universitat de Barcelona, Martí i Franquès 1, 08028 Barcelona, Spain.
E-mail: f.calle.vallejo@ub.edu

[b] Qi Hang Low and Dr. Boon Siang Yeo
Department of Chemistry, Faculty of Science, National University of Singapore, 3 Science Drive 3, Singapore 117543 and the Solar Energy Research Institute of Singapore, SERIS, National University of Singapore (NUS), 7 Engineering Drive 1, Building E3A, #06-01, Singapore 117574.
E-mail: chmyeos@nus.edu.sg

[c] Dr. Albertus D. Handoko
Institute of Materials Research and Engineering, Agency for Science, Technology and Research (A*STAR), 2 Fusionopolis Way, Innovis, Singapore 138634, Singapore.

Supporting information for this article is given via a link at the end of the document.

Abstract: The electrochemical CO and CO_2 reduction reactions (CORR and CO_2RR) using copper catalysts and renewable electricity hold promise as a carbon-neutral route to produce commodity chemicals and fuels. However, the exact mechanisms and structure sensitivity of Cu electrodes toward C_2 products are still under debate. Herein, we investigate ethylene oxide reduction (EOR) as a proxy to the late stages of CORR to ethylene, and the results are compared to those of acetaldehyde reduction to ethanol. DFT calculations show that ethylene oxide undergoes ring opening before exclusively reducing to ethylene via *OH formation. A selectivity map for the late stages of CORR and CO_2RR based on generalized coordination numbers ($\overline{CN}$) shows that sites with moderate coordination ($5.9 < \overline{CN} < 7.5$) are efficient for ethylene production, with pristine Cu(100) being more active than defective surfaces such as Cu(311). In contrast, kinks and edges are more active for ethanol production, and (111) terraces are relatively inert.

Introduction

The electrochemical reduction of carbon monoxide and carbon dioxide (CORR and CO_2RR) using solar electricity has the potential to supply useful chemicals and liquid fuels sustainably while maintaining carbon neutrality.[1,2,3] Pioneering works from Hori and coworkers showed that copper is a unique catalyst capable of catalyzing the production of a variety of hydrocarbons and alcohols from CORR[4] and CO_2RR.[5] Interestingly, the relative abundance of certain products depends strongly on the catalyst's morphology and the applied potential. Specifically, methane tends to abound when Cu electrodes have hexagonal symmetry (e.g. pristine and stepped Cu(111)) (see Figure 1a for the side view of different facets). On the other hand, electrodes with square symmetry, for example Cu(100), favor C_2 products such as ethylene and ethanol. Additionally, methane evolution commences at considerably more negative potentials than those required to form C_2 compounds.[6,7,8,9] Such dissimilar behavior indicates that the C_1 and C_2 reaction pathways are likely mediated by different species.

The C_2 pathways seem to proceed via several common intermediates, as evidenced by the experimental observation that the Faradaic efficiencies of ethylene and ethanol shift similarly when different alkaline cations are used in the electrolyte.[10] Ethylene and ethanol are also known to have identical or similar onset potentials,[11,12,13] which suggests that they share a common potential-limiting step. Further insight can be extracted from the pH independence in the standard hydrogen electrode (SHE) scale of the CORR to ethylene and ethanol.[4] This observation suggests that C-C bonds are made via CO coupling through an electron transfer followed by a proton transfer.

Indeed, computational studies have indicated that during CORR on Cu(100) to C_2 species, the coupling of two *CO mediated by an electron transfer to form $*C_2O_2^-$ is potential-limiting.[14] Besides, ethylene and ethanol were found to share the same intermediates up to the fifth proton-electron transfer. The pathways to ethanol and ethylene then bifurcate, with the latter being the dominant product on that facet. To improve the selectivity toward acetaldehyde and ethanol, modified Cu catalysts such as oxide-derived Cu (OD-Cu)[15,16,17,18] or CuAg composites have been used.[19,20,21,22]

The intermediate formed upon the fifth proton-electron transfer in the C_2 pathway during CORR is $*CH_2CHO$. If the alpha carbon is hydrogenated, acetaldehyde (CH_3CHO) is produced. This molecule has been experimentally detected as a CORR intermediate on OD-Cu,[15] and shown to reduce entirely to ethanol on Cu electrodes.[23] If the carbonyl carbon is hydrogenated, adsorbed oxygen (*O) and gaseous ethylene are formed ($*CH_2CHO + H^+ + e^- \rightarrow *O + C_2H_{4(g)}$).[14] A closer inspection of the latter electrochemical step shows that it convolutes the hydrogenation of the carbonyl carbon and the scission of the C-O bond. As the kinetic barrier for the scission has been shown to be large,[24,25] $*OCH_2CH_2$ might form at the surface of the electrodes. Such an oxametallacycle species, known in gas-phase heterogeneous catalysis,[26] is a bidentate, adsorbed form of ethylene oxide in which the epoxy ring has opened (see schematics in Figure 1b). Thus, the final stages of CO_2RR and CORR to ethylene on Cu may be regarded as the electrochemical ethylene oxide reduction (EOR).[7]

A previous study by Schouten et al. showed this possibility when they examined various possible precursors to ethylene, such as glyoxal, glycolaldehyde, ethylene glycol and ethylene oxide. They found that only ethylene oxide was reduced to ethylene on polycrystalline Cu.[7] Additionally, they showed that the onset potential for the EOR occurs earlier on Cu(100) as compared to Cu(111), which indicates that EOR is more efficiently catalyzed by Cu(100).[27] This observation agrees with the results for CO2RR and CORR, where ethylene forms on Cu(100) with lower onset potentials than on Cu(111).[1,3,11,27] It has been hypothesized that the reason behind the lower EOR onset potential on Cu(100) is the enhanced stability of the oxametallacycle intermediate from ethylene oxide reduction on this surface.[7] Given that some intermediates are possibly shared, but ethylene is usually more abundantly produced than ethanol during CO_2RR and CORR,[28] it is critical to understand what drives the functionality of Cu catalysts toward specific C_2 molecules.

Herein, we provide a computational-experimental study of EOR to ethylene on copper electrodes. The onset potentials for ethylene formation were determined for Cu(111), Cu(100), Cu(211) and Cu(311) single-crystal electrodes. We find a quantitative correlation between the experimental and calculated onset potentials and the geometric structure of the active sites. Furthermore, we elucidate the most likely reaction pathway for EOR to ethylene, where *OH protonation is the potential-limiting step for all the studied surface sites. More importantly, we build a selectivity map for the late stages of CO_2RR and CORR to C_2 products at Cu surfaces. The chart shows how the selectivity toward either ethanol or ethylene is modulated by the geometric structure of the active sites.

Results and Discussion

1. Active sites and reaction pathways. The pathways through which ethylene oxide may be reduced to either ethylene ($C_2H_4O_{(g)} + 2H^+ + 2e^- \rightarrow C_2H_{4(g)} + H_2O_{(l)}$) or ethanol ($C_2H_4O_{(g)} + 2H^+ + 2e^- \rightarrow C_2H_5OH_{(l)}$) via 2-electron catalytic processes are shown in Figure 1b. We studied the possible pathways on Cu(100), Cu(111) and four defective Cu surfaces, namely, Cu(211), Cu(311), 4AD@Cu(100) (four Cu adatoms on Cu(100)) and 4AD@Cu(111) (four Cu adatoms on Cu(111)). A depiction of the different active sites under study is shown in Figure 1a and the calculated adsorption energies appear in Table S10 in the Supporting Information (SI). We concluded that the most favorable pathway in all cases is the one that leads to ethylene via Equations 1 to 3 (green pathway in Figure 1b).

$$C_2H_4O_{(g)} + * \rightarrow *OCH_2CH_2 \quad (1)$$

$$*OCH_2CH_2 + H^+ + e^- \rightarrow *OH + C_2H_{4(g)} \quad (2)$$

$$*OH + H^+ + e^- \rightarrow H_2O_{(l)} \quad (3)$$

where * is a free surface site. The first step is the chemisorption of ethylene oxide, which involves the opening of the epoxy ring and a bidentate adsorption configuration (Equation 1). Ethylene and *OH are formed after the first proton-electron transfer (Equation 2). Finally, *OH is reduced to $H_2O_{(l)}$ upon the second proton-electron transfer, such that the active site is free again to start a new catalytic cycle (Equation 3).

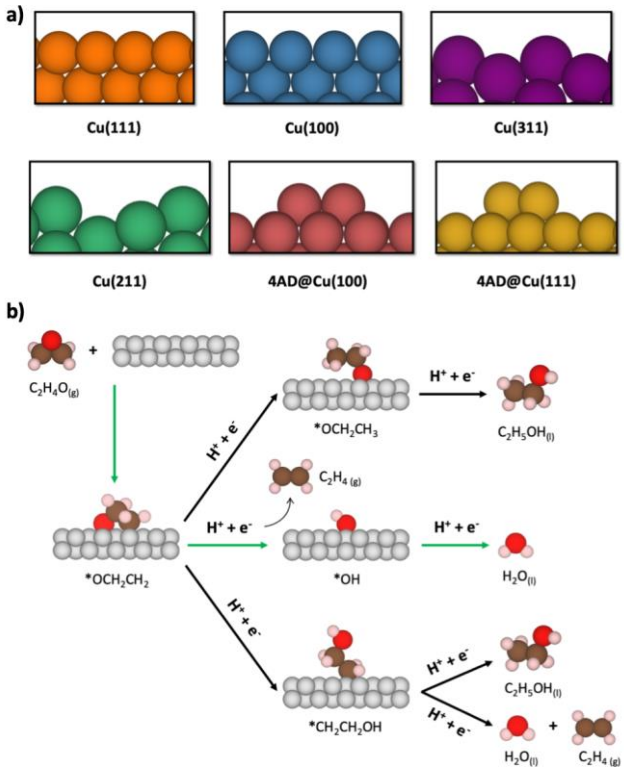

Figure 1. a) Side views of the surface models used in this work. b) Schematics of the different reaction pathways for ethylene oxide reduction to ethylene and ethanol on Cu electrodes. The first step is the chemisorption of ethylene oxide, whereas the other steps are electrochemical. The green arrows mark the lowest-energy pathway. Cu, C, O and H atoms are shown in gray, brown, red and pink, respectively.

It is important to note that if a given site does not bind ethylene oxide strong enough (Equation 1), it would be difficult for EOR to proceed. This could occur as a result of the competitive adsorption of *H, which is involved in the hydrogen evolution reaction. Hence, before we analyze the electrochemical steps in Equations 2 and 3, a comparison between hydrogen and ethylene oxide adsorption is necessary. The adsorption energies are plotted in Figure 2 as a function of the generalized coordination number ($\overline{CN}$) of the active sites (see Section S7 in the SI for the details on the assessment of $\overline{CN}$). *H and $*OCH_2CH_2$ behave differently, as only the latter displays strong structural sensitivity. Interestingly, we found that the adsorption energies of *H and $*OCH_2CH_2$ are comparable on Cu(111) terrace sites. Consequently, Cu(111) will probably have a higher *H coverage as compared to the other Cu facets, since these latter surfaces adsorbed $*OCH_2CH_2$ more strongly than *H. As ethylene oxide adsorption requires binding to several surface atoms, its adsorption is likely hindered to a large extent by the high coverage of *H on Cu(111).

Furthermore, we note that the adsorption energy of ethylene oxide on Cu(100) noticeably departs from the linear trend in Figure 2. As $*OCH_2CH_2$ is a bidentate adsorbate, this departure can be attributed to the ensemble effects originating from its double-bridge adsorption configuration (shown in Figure S7 of the SI), in line with previous reports for similar bidentate adsorbates at square-symmetry sites.[29,30] According to those works, ensemble effects should generally be present on (100)-like sites but tend to be less pronounced at undercoordinated sites. Indeed, we observe just that for 4AD@Cu(100) in Figure 2, whereby the deviation from the linear trend is within a confidence interval of 83% set at ±2 MAE (MAE: mean absolute error).

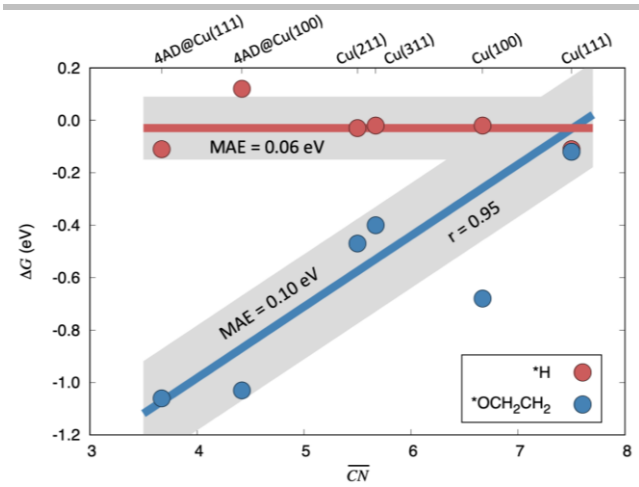

Figure 2. Adsorption free energies of $*OCH_2CH_2$ (in blue, see Equation 1) and *H (in red, with respect to $H^+ + e^-$) as a function of the generalized coordination number ($\overline{CN}$) of the active sites. A linear regression for $*OCH_2CH_2$ along with the corresponding Pearson correlation coefficient is shown, without including Cu(100) in view of its known ensemble effects.[29,30] The red line is the arithmetic mean of the *H adsorption energies. A grey band of ±2 MAE is provided around the lines. MAE: mean absolute error of the points with respect to the linear fit.

2. Experimental and computational onset potentials. The free-energy diagrams with the relative stability of the reaction intermediates in Equations 1 to 3 for the six surface models under study are shown in Figure S8. In Figure 3a, we condense all those data in the form of a coordination-activity plot, in which the limiting potential for each site is correlated with its respective generalized coordination number. All sites share the same potential-limiting step, namely *OH hydrogenation to H_2O (Equation 3). The calculated onset potentials for Cu(111), Cu(100), Cu(311), Cu(211), 4AD@Cu(100) and 4AD@Cu(111) are respectively -0.04, -0.34, -0.46, -0.50, -0.48, and -0.52 V vs RHE.

Next, we determined experimentally the onset potentials for EOR on copper surfaces (see Figure 3 and Table S2). The reaction was performed at pH = 7 in 0.1 M potassium phosphate buffer electrolyte. An electrolyte with neutral pH was chosen to avoid the side reactions of ethylene oxide to give ethylene glycol and polyethylene glycol under acidic and basic conditions.[31] The surfaces of the Cu electrodes used were characterized using cyclic voltammetry and X-ray diffraction (XRD) (Figures S1-S4). During electrolysis, ethylene oxide (2.5 mol % in N_2 gas balance) was constantly bubbled into the cathodic compartment. The EOR products were identified by gas and liquid chromatography. Ethylene was the only EOR product detected and ethanol was not observed, even at considerably more negative potentials, namely -1 V vs RHE (Figure S6). This agrees with the DFT results, which show that ethylene is the more favorable EOR product (Figure 1 and Table S10).

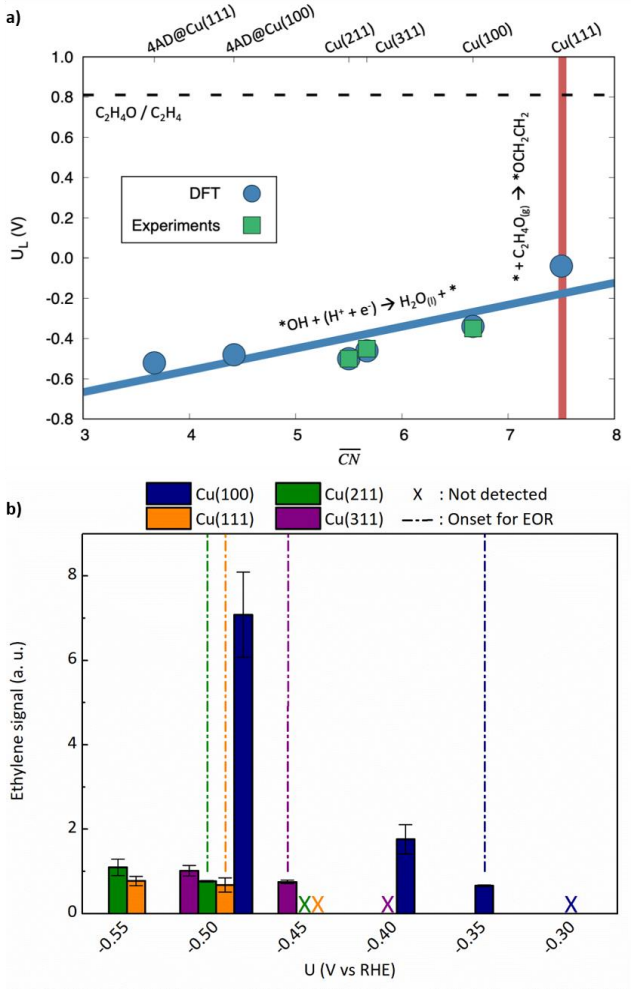

Figure 3. a) Coordination-activity plot for ethylene oxide reduction to ethylene. The calculated (blue) and measured (green) onset potentials are plotted as a function of generalized coordination numbers ($\overline{CN}$) for various electrodes. The dashed line is the equilibrium potential (0.81 V vs RHE) and the red line marks the separating point, whereby *OCH_2CH_2 adsorbs more strongly than *H for surfaces with $\overline{CN}$ on the left side of the red line. Detailed free-energy diagrams are provided in Figure S8. b) Ethylene signals during EOR on Cu(111), Cu(100), Cu(311), and Cu(211) at different applied potentials in 0.1 M potassium phosphate buffer solution (pH = 7). X marks the potentials where ethylene evolved from EOR was not in detectable amounts.

The experimental EOR onset potential was determined to be the potential at which the ethylene signal begins to be stronger than the baseline signal (see Section S3 in the SI). The onset potentials for Cu(100) and Cu(111) were -0.35 and -0.50 V vs RHE respectively (Figure 3b). Compared to the calculated values of -0.34 and -0.04 V vs RHE on these two surfaces, it is striking that there is only good agreement for Cu(100). Judging by the simulated onset potentials for four defective surfaces, which are all in the narrow range of -0.46 to -0.52 V vs RHE (Figure 3a), we hypothesized that the discrepancy could stem from the fact that defects on the Cu(111) crystal, rather than the Cu(111) terraces themselves, catalyze the EOR.

We evaluated this hypothesis by performing EOR on Cu(211) and Cu(311). These two surfaces have respectively 3-atom- and 2-atom-wide (111) terraces, separated by monoatomic (100) steps. The experimental EOR onset potential on Cu(211) was -0.50 V vs RHE (Figure 3b), which is the same as that of Cu(111). For Cu(311), the EOR onset potential, which was at -0.45 V vs RHE, was slightly earlier than that on Cu(211) and Cu(111) (Figure 3b). This result is in good agreement with the presence of a higher density of step edges on Cu(311), which can increase the amount of ethylene formed from EOR, thus resulting in a somewhat earlier EOR onset. Overall, similar onset potentials were determined for Cu(111), Cu(211) and Cu(311), which strongly indicates that the 'discrepancy' between the experimental and calculated onset of EOR on Cu(111) was due to (i) the presence of defective sites such as step edges, and (ii) the inability of Cu(111) to sustain an appreciable coverage of adsorbed ethylene oxide.

In this context, the ethylene signals obtained on the different facets at -0.50 V vs RHE are noteworthy (Figure 3b): Cu(100) produces the highest amount of ethylene from EOR amongst all the facets studied, followed by Cu(311), Cu(211) and lastly on Cu(111). This finding further highlights the importance of (100) facets for the EOR to ethylene and the fact that (111) terraces are likely inactive. This conclusion goes along the same lines of previous studies for similar organic reactions, e.g. acetone reduction, where (111) terraces were also observed to be rather inactive in view of the competition of the adsorbates with *H for adsorption sites at potentials close to 0 V vs RHE.[23,32,33,34]

3. Implications for CO_2RR and CORR. Numerous works on roughened and oxide-derived Cu catalysts have invoked the presence of step and defect sites as being responsible for enhanced ethylene formation from CO_2RR or CORR.[35,36,37] Our experimental and computational onset potentials in Figure 3 suggest that this general claim is likely inaccurate, as Cu(311), which has abundant step edges, actually catalyzed ethylene formation less readily than Cu(100). This observation also concurs with a previous work on CuCl-derived Cu mesocrystals.[38] The surfaces of these catalysts, which consist mainly of various atomic steps and (100) terraces, reduced CO_2 to ethylene more selectively than Cu nanoparticles. Unlike the Cu mesocrystals, the Cu nanoparticle surface were found to have high-index planes composed of abundant steps, but with no terraces. The present results further stress the importance of Cu(100) terraces for the selective formation of ethylene during CO_2 electrolysis.

The standard potential for the reduction of ethylene oxide to ethylene is 0.81 V vs RHE. Judging by the calculated and measured onset potentials, we conclude that, despite its apparent simplicity, the EOR on Cu requires large overpotentials of no less than ~1.15 V. Knowing that Equation 3 ($*OH + H^+ + e^- \rightarrow H_2O_{(l)}$) is the potential-limiting step for all the studied models (See Figure 3a), destabilizing *OH would likely lead to lower overpotentials. Different strategies may be used to this end, for example, changing Cu-Cu distances via strain,[39,40,41] making use of different electrolytes so that cation and/or anion effects modify *OH adsorption energies,[42,43] and using nonaqueous solvents such as acetonitrile to avoid the stabilization granted by *OH-H_2O hydrogen bonds.[44,45] These strategies are also important for the CORR to ethylene on Cu(100), as the onset potential is around -0.40 V vs RHE and is usually attributed to the formation of a CO dimer.[11,14] Once the dimer formation is experimentally optimized so as to require a significantly less negative potential, the next target will probably be *OH, as its conversion to H_2O requires -0.35 V vs RHE according to Figure 3.

Finally, we will compare the EOR results to those of the acetaldehyde reduction reaction (ARR) on Cu.[23] Experimentally, the ARR leads exclusively to ethanol ($CH_3CHO_{(l)} + 2H^+ + 2e^- \rightarrow C_2H_5OH_{(l)}$) and its equilibrium potential is 0.24 V vs RHE. On Cu electrodes, the ARR is limited by the formation of a monodentate, O-bound ethoxy intermediate ($* + CH_3CHO_{(l)} + H^+ + e^- \rightarrow *OCH_2CH_3$), the hydrogenation of which is usually downhill in energy to produce ethanol ($*OCH_2CH_3 + H^+ + e^- \rightarrow * + C_2H_5OH_{(l)}$).

In Figure 4a, we provide a selectivity map of Cu sites for the ARR, EOR and hydrogen evolution reaction (HER). The plot connects the generalized coordination of the active sites to the preferred reaction products and limiting potentials (U_L). ARR is thermodynamically more favorable than EOR at highly undercoordinated Cu sites ($\overline{CN} < 5.9$), that are characteristic of step edges and kinks. Note that this result helps to explain why in a recent work, Cu_3 and Cu_4 clusters could reduce CO_2 to ethanol with Faradaic efficiencies of up to 91%.[46] On the other hand, ethylene formation is favorable at moderate-coordination sites ($5.9 < \overline{CN} < 7.5$). Cu(100) terraces belong to this category and introducing undercoordinated defects onto facets within this category makes the limiting potential more negative. This is what we observed experimentally in Figure 3b. Finally, adsorbed hydrogen prevails over adsorbed ethylene oxide on Cu(111) terraces and more coordinated sites ($\overline{CN} > 7.5$), which renders them inactive for the EOR. This is also in line with the experimental results shown in Figure 3b.

We note in Figure 4a that the opposite slopes for the right leg of ARR (in blue, $3.7 < \overline{CN} < 5.9$) and the EOR region (in green, $5.9 < \overline{CN} < 7.5$) suggest that undercoordination has opposite effects on the catalytic activities. Interestingly, these observations coincide with many previous findings for CO_2RR and CORR: (I) Pristine Cu(100) is usually selective toward ethylene.[6,27,28] (II) A rougher Cu surface, which intuitively is a surface with more defective sites such as steps and kinks, will enhance the relative production of ethanol over ethylene as compared to smoother Cu surfaces, as illustrated in Figure 4b and Section S4 in the SI.[13,16,47-50] (III) Cu(111) produces low amounts of C_2 species.[6,27,28] In this order of ideas, electrodes where a multiplicity of sites coexist, will likely lead to a mix of C_2 products as a result of CO_2RR and CORR.

Conclusion

Despite extensive research on CO_2RR and CORR, there is not yet a consensus about the complete reaction mechanism. Herein, we studied the ethylene oxide reduction (EOR) as a proxy for the late stages of the CO_2RR and CORR pathway to ethylene on Cu. *OH hydrogenation is the potential-limiting step in all studied cases, and the most efficient surface for EOR is Cu(100), with an onset potential of -0.35 V vs RHE. The EOR onsets for Cu(111) and Cu(211) were identical at -0.50 V vs RHE, but the measured current densities were smaller on the former, suggesting that only defect sites on Cu(111) are active.

Comparing the acetaldehyde reduction reaction (ARR) to EOR on Cu, we conclude that the former is favored at highly undercoordinated sites ($\overline{CN} < 5.9$, typical of step edges and kinks); the latter is preferred at moderately undercoordinated sites ($5.9 < \overline{CN} < 7.5$, e.g. Cu(100)); and hydrogen adsorption precludes ethylene oxide on Cu(111) and more coordinated sites ($\overline{CN} > 7.5$).

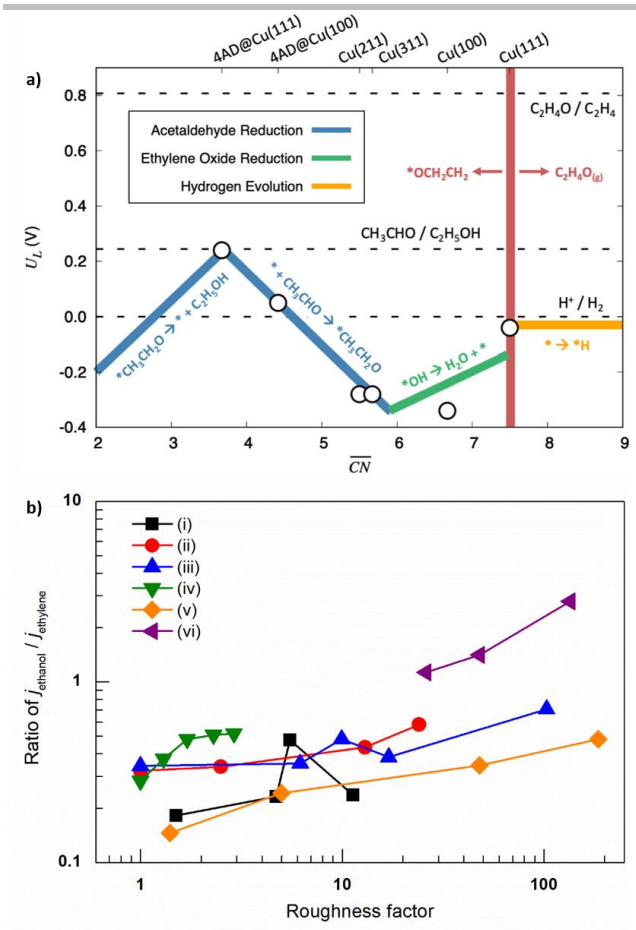

Figure 4. a) Selectivity map for the late stages of CO and CO_2 electroreduction on Cu electrodes. The calculated limiting potentials (U_L) are plotted as a function of the generalized coordination number ($\overline{CN}$) of the active sites. The upper x-axis shows the studied active sites. Acetaldehyde reduction (blue) to ethanol is most favorable on low-coordination sites ($\overline{CN} < 5.9$), whereas ethylene oxide reduction (green) to ethylene is most favorable on intermediate-coordination sites ($5.9 < \overline{CN} < 7.5$). For $\overline{CN} > 7.5$, only hydrogen evolution (orange) proceeds. To the left of the red line ($\overline{CN} = 7.5$), the catalytic sites adsorb ethylene oxide more strongly than *H. The dashed lines mark the equilibrium potentials; the potential-limiting steps are provided in each case. b) Ratio of $j_{ethanol}$ / $j_{ethylene}$ of various Cu catalysts plotted as a function of catalysts' roughness factor. All data used are obtained from previous CO_2RR (i-v) or CORR (vi) studies (Section S4 in the SI): (i) reference 13, (ii) reference 47, (iii) reference 48, (iv) reference 49, (v) reference 50, (vi) reference 16.

In broader terms, our findings indicate that the most active sites for CO_2RR and CORR are different for each C_2 product: Cu(100) terraces favor ethylene formation, whilst steps, kinks and akin undercoordinated defects favor ethanol evolution. As the EOR and the ARR lead exclusively to ethylene and ethanol, respectively, we conclude that the lack of CO_2RR selectivity on Cu stems from surface inhomogeneities and is dictated by the site-specific formation of either $*OCH_2CH_2$ or CH_3CHO.

Acknowledgements

F.C.-V acknowledges funding from Spanish MICIUN RTI2018-095460-B-I00 and María de Maeztu MDM-2017-0767 grants and partly by Generalitat de Catalunya 2017SGR13. O.P. thanks the Spanish MICIUN for a PhD grant (PRE2018-083811). We thank Red Española de Supercomputación (RES) for supercomputing time at SCAYLE (projects QS-2019-3-0018, QS-2019-2-0023, and QCM-2019-1-0034), MareNostrum (project QS-2020-1-0012), and CENITS (project QS-2020-2-0021). The use of supercomputing facilities at SURFsara was sponsored by NWO Physical Sciences, with financial support by NWO. Q.H.L and BSY acknowledge funding from the National University of Singapore (R-143-000-B52-114 and R-143-000-A64-114), National University of Singapore Flagship Green Energy Program (R-143-000-A55-733 and R-143-000-A55-646), and the Solar Energy Research Institute of Singapore (SERIS).

Keywords: Density functional theory • Carbon dioxide reduction • Electrocatalysis • Ethylene oxide reduction • Copper single crystals surfaces

[1] S. Nitopi, E. Bertheussen, S. B. Scott, X. Liu, A. K. Engstfeld, S. Horch, B. Seger, I. E. L. Stephens, K. Chan, C. Hahn, J. K. Nørskov, T. F. Jaramillo, I. Chorkendorff, Chem. Rev. 2019, 119, 7610–7672.
[2] O. S. Bushuyev, P. D. Luna, C. T. Dinh, L. Tao, G. Saur, J. van de Lagemaat, S. O. Kelley, E. H. Sargent, Joule 2018, 2, 825–832.

[3] Y. Y. Birdja, E. Pérez-Gallent, M. C. Figueiredo, A. J. Göttle, F. Calle-Vallejo, M. T. M. Koper, Nat. Energy 2019, 4, 732–745.
[4] Y. Hori, R. Takahashi, Y. Yoshinami, A. Murata, J. Phys. Chem. B 1997, 101, 7075–7081.
[5] Y. Hori, H. Wakebe, T. Tsukamoto, O. Koga, Electrochimica Acta 1994, 39, 1833–1839.
[6] K. J. P. Schouten, Z. Qin, E. Pérez Gallent, M. T. M. Koper, J. Am. Chem. Soc. 2012, 134, 9864–9867.
[7] K. J. P. Schouten, Y. Kwon, C. J. M. van der Ham, Z. Qin, M. T. M. Koper, Chem. Sci. 2011, 2, 1902–1909.
[8] G. L. De Gregorio, T. Burdyny, A. Loiudice, P. Iyengar, W. A. Smith, R. Buonsanti, ACS Catal. 2020, 10, 4854–4862.
[9] Y. Huang, A. D. Handoko, P. Hirunsit, B. S. Yeo, ACS Catal. 2017, 7, 1749–1756.
[10] A. Murata, Y. Hori, Bull. Chem. Soc. Jpn. 1991, 64, 123–127.
[11] E. Pérez-Gallent, G. Marcandalli, M. C. Figueiredo, F. Calle-Vallejo, M. T. M. Koper, J. Am. Chem. Soc. 2017, 139, 16412–16419.
[12] K. P. Kuhl, E. R. Cave, D. N. Abram, T. F. Jaramillo, Energy Environ. Sci. 2012, 5, 7050–7059.
[13] D. Ren, Y. Deng, A. D. Handoko, C. S. Chen, S. Malkhandi, B. S. Yeo, ACS Catal. 2015, 5, 2814–2821.
[14] F. Calle‐Vallejo, M. T. M. Koper, Angew. Chem. Int. Ed. 2013, 52, 7282–7285.
[15] E. Bertheussen, A. Verdaguer‐Casadevall, D. Ravasio, J. H. Montoya, D. B. Trimarco, C. Roy, S. Meier, J. Wendland, J. K. Nørskov, I. E. L. Stephens, I. Chorkendorff, Angew. Chem. Int. Ed. 2016, 55, 1450–1454.
[16] C. W. Li, J. Ciston, M. W. Kanan, Nature 2014, 508, 504–507.
[17] Y. Lum, J. W. Ager, Nat. Catal. 2019, 2, 86–93.
[18] O. Piqué, F. Viñes, F. Illas, F. Calle-Vallejo, ACS Catal. 2020, 10, 10488–10494.
[19] L. R. L. Ting, O. Piqué, S. Y. Lim, M. Tanhaei, F. Calle-Vallejo, B. S. Yeo, ACS Catal. 2020, 10, 4059–4069.
[20] E. L. Clark, C. Hahn, T. F. Jaramillo, A. T. Bell, J. Am. Chem. Soc. 2017, 139, 15848–15857.
[21] L. Wang, D. C. Higgins, Y. Ji, C. G. Morales-Guio, K. Chan, C. Hahn, T. F. Jaramillo, Proc. Natl. Acad. Sci. 2020, 117, 12572–12575.
[22] D. Higgins, A. T. Landers, Y. Ji, S. Nitopi, C. G. Morales-Guio, L. Wang, K. Chan, C. Hahn, T. F. Jaramillo, ACS Energy Lett. 2018, 3, 2947–2955.
[23] I. Ledezma-Yanez, E. P. Gallent, M. T. M. Koper, F. Calle-Vallejo, Catal. Today 2016, 262, 90–94.
[24] W. Luo, X. Nie, M. J. Janik, A. Asthagiri, ACS Catal. 2016, 6, 219–229.
[25] D. Torres, N. Lopez, F. Illas, R. M. Lambert, J. Am. Chem. Soc. 2005, 127, 10774–10775.
[26] S. Linic, M. A. Barteau, J. Am. Chem. Soc. 2002, 124, 310–317.
[27] K. J. P. Schouten, E. Pérez Gallent, M. T. M. Koper, ACS Catal. 2013, 3, 1292–1295.
[28] Y. Hori, I. Takahashi, O. Koga, N. Hoshi, J. Mol. Catal. Chem. 2003, 199, 39–47.
[29] H. Li, F. Calle-Vallejo, M. J. Kolb, Y. Kwon, Y. Li, M. T. M. Koper, J. Am. Chem. Soc. 2013, 135, 14329–14338.
[30] H. Li, Y. Li, M. T. M. Koper, F. Calle-Vallejo, J. Am. Chem. Soc. 2014, 136, 15694–15701.
[31] G. A. Melhem, A. Gianetto, M. E. Levin, H. G. Fisher, S. Chippett, S. K. Singh, P. I. Chipman, Process Saf. Prog. 2001, 20, 231–246.
[32] C. J. Bondue, F. Calle-Vallejo, M. C. Figueiredo, M. T. M. Koper, Nat. Catal. 2019, 2, 243–250.
[33] Y.-J. Zhang, V. Sethuraman, R. Michalsky, A. A. Peterson, ACS Catal. 2014, 4, 3742–3748.
[34] Z. P. Jovanov, H. A. Hansen, A. S. Varela, P. Malacrida, A. A. Peterson, J. K. Nørskov, I. E. L. Stephens, I. Chorkendorff, J. Catal. 2016, 343, 215–231.
[35] Y. Hori, I. Takahashi, O. Koga, N. Hoshi, J. Phys. Chem. B 2002, 106, 15–17.
[36] W. Tang, A. A. Peterson, A. S. Varela, Z. P. Jovanov, L. Bech, W. J. Durand, S. Dahl, J. K. Nørskov, I. Chorkendorff, Phys. Chem. Chem. Phys. 2012, 14, 76–81.
[37] R. Kas, R. Kortlever, A. Milbrat, M. T. M. Koper, G. Mul, J. Baltrusaitis, Phys. Chem. Chem. Phys. 2014, 16, 12194–12201.
[38] C. S. Chen, A. D. Handoko, J. H. Wan, L. Ma, D. Ren, B. S. Yeo, Catal. Sci. Technol. 2014, 5, 161–168.
[39] F. Calle-Vallejo, A. S. Bandarenka, ChemSusChem 2018, 11, 1824–1828.
[40] A. Khorshidi, J. Violet, J. Hashemi, A. A. Peterson, Nat. Catal. 2018, 1, 263–268.
[41] M. Escudero-Escribano, P. Malacrida, M. H. Hansen, U. G. Vej-Hansen, A. Velázquez-Palenzuela, V. Tripkovic, J. Schiøtz, J. Rossmeisl, I. E. L. Stephens, I. Chorkendorff, Science 2016, 352, 73–76.
[42] B. Garlyyev, S. Xue, M. D. Pohl, D. Reinisch, A. S. Bandarenka, ACS Omega 2018, 3, 15325–15331.
[43] K. Holst-Olesen, M. Reda, H. A. Hansen, T. Vegge, M. Arenz, ACS Catal. 2018, 8, 7104–7112.
[44] A. Fortunelli, W. A. Goddard, Y. Sha, T. H. Yu, L. Sementa, G. Barcaro, O. Andreussi, Angew. Chem. Int. Ed. 2014, 53, 6669–6672.
[45] F. Calle-Vallejo, A. Krabbe, J. M. García-Lastra, Chem. Sci. 2017, 8, 124–130.
[46] H. Xu, D. Rebollar, H. He, L. Chong, Y. Liu, C. Liu, C.-J. Sun, T. Li, J. V. Muntean, R. E. Winans, D.-J. Liu, T. Xu, Nat. Energy 2020, 5, 623–632.
[47] D. Ren, N. T. Wong, A. D. Handoko, Y. Huang, B. S. Yeo, J. Phys. Chem. Lett. 2016, 7, 20–24.
[48] Y. Lum, B. Yue, P. Lobaccaro, A. T. Bell, J. W. Ager, J. Phys. Chem. C 2017, 121, 14191–14203.
[49] Y. Kwon, Y. Lum, E. L. Clark, J. W. Ager, A. T. Bell, ChemElectroChem 2016, 3, 1012–1019.
[50] D. Ren, J. Fong, B. S. Yeo, Nat. Commun. 2018, 9, 925.